Frontiers of Optoelectronics (2022) 15:4
https://doi.org/10.1007/s12200-022-00007-6

Frontiers of Optoelectronics

RESEARCH ARTICLE

Spatial beam reshaping and large-band nonlinear conversion in rectangular-core phosphate glass fibers

Clément Strutynski[1] · Vincent Couderc[2] · Tigran Mansuryan[2] · Giorgio Santarelli[3] · Philippe Thomas[2] · Sylvain Danto[1] · Thierry Cardinal[1]

Received: 28 May 2021 / Accepted: 7 September 2021

Abstract
Here we present the ability of Nd^{3+}-doped zinc-phosphate glasses to be shaped into rectangular core fibers. At first, the physico-chemical properties of the developed P_2O_5-based materials are investigated for different concentrations of neodymium oxide and core and cladding glass compositions are selected for further fiber development. A modified stack-and-draw technique is used to produce multimode large rectangular-core optical fibers. Self-guided nonlinear effects acting as spatial beam reshaping processes occurring in these newly-developed photonic structures lead to the generation of spectral broadenings in the visible and near-infrared spectral domains.

Keywords Phosphate glasses · Neodymium · Optical fibers · Self-focusing · Super-continuum

1 Introduction

Multimode graded index optical fibers have recently received strong interest because of their ability to transform a multimode propagation into a quasi-single mode one. This effect, called spatial self-cleaning, is based on four-wave mixing (FWM) process, which is phase matched by a longitudinal grating formed by the interplay between a spatial self-imaging and the Kerr effect [1]. Thus, high peak power can be guided in multimode fibers without significant spatial spreading of the energy in a speckled beam. Combined with special active rare-earth doped gain media, the exploitation of such dynamics has proven promising for the power scaling of all-fibered laser sources [2]. Alternatively, nonlinear spatial cleaning of multimode beams can advantageously provide strong power density inside the waveguiding structure and lead to supercontinuum (SC) generation [3, 4]. Broadband generation by using nonlinear conversions was first introduced in 1970 by Alfano and Shapiro in bulk glass [5]. Later, the advent of microstructured optical fibers, in the 1990s [6], attracted new interest, guided by the design of the curve dispersion of nonlinear fibers. Thus, the control of nonlinear processes at the origin of the supercontinuum generation has been possible. Broadband lasers became the usual sources for many applications, such as nonlinear fluorescence imaging and multispectral Lidar. Pulsed laser sources ranging from femtosecond [5] to nanosecond [7] have been used without forgetting the continuous wave (CW) regime [8]. Detailed explanations of nonlinear processes involved in supercontinuum generation can be found in the paper published by Dudley et al. in 2006 [9]. Up to now, graded index optical fibers have been the main photonic structures which can support spatial self-cleaning processes. However, it is interesting to underline that non-cylindrical fiber geometries can also be considered to transfer power, propagating on the fundamental mode toward higher-order modes (HOMs), by exploiting nonlinear dynamics [10]. Besides, linear and cubic nonlinear imaging effects were experimentally investigated in slab waveguides [11]. Building on this, it appears that the development of rectangular fibers provides very interesting features for nonlinear spatial

Clément Strutynski is now part of the Laboratoire Interdisciplinaire Carnot de Bourgogne (ICB), UMR6303 CNRS – Université Bourgogne Franche-Comté, 21000 Dijon, France

✉ Sylvain Danto
sylvain.danto@u-bordeaux.fr

[1] Institute of Chemistry of the Condensed Matter of Bordeaux (ICMCB), Chemistry Department, 33608 Pessac, France

[2] UMR CNRS 7252, Université de Limoges, XLIM, 87060 Limoges, France

[3] LP2N, Institut d'Optique Graduate School– CNRS– University of Bordeaux, 33400 Talence, France

Published online: 29 March 2022

reshaping effects and for frequency conversion [12, 13]. These unique structures were initially investigated on silicate glasses for their better thermal management and pump absorption efficiency. They can, however, be designed from other materials exhibiting more suitable assets for laser applications, such as phosphate glasses. P_2O_5-based materials provide high solubility of rare-earth ions, up to several 10^{20} ions/cm^3, good chemical durability, excellent optical properties and fiber-shaping ability [14, 15]. Previous studies have indicated that they overcome several silica-related limitations (photo darkening, Brillouin scattering, etc.) in the domain of fiber [16–20]; shorter [21–23] or high power [24, 25] fibered laser configurations are already available with these glasses. As an illustration, Nd^{3+}-doped metaphosphate has been extensively investigated for the development of high energy and high-peak-power laser applications such as the multi-kilojoule, multi-terawatt lasers for fusion energy research ignition facilities [26]. Recently, a single-frequency laser operation in the 900 nm wavelength range with an output power of 13.5 mW has been demonstrated using an Nd^{3+}-doped phosphate fiber as the gain medium [27].

In this paper, we present an overview of the fabrication process and characterization of Nd-doped zinc-phosphate rectangular-core step-index fibers. First, the effect of Nd_2O_3 addition on the physicochemical properties of the glass $55P_2O_5$–$30ZnO$–$10K_2O$–$5Al_2O_3$ is studied. Thermal and optical properties show linear evolution with respect to the Nd^{3+} concentration, allowing fine control of the glass transition temperature and of the refractive index. Core and cladding glasses were selected based on these investigations and a rectangular-core multimode optical fiber was manufactured using a modified stack-and-draw technique recently developed by our group [28]. Thereafter, femtosecond laser pumping was employed to demonstrate the generation of a large-band spectral broadening in these newly-developed fibers thanks to self-guided nonlinear effects.

2 Experimental procedure

2.1 Glass preparation

Phosphates glasses of composition $(55P_2O_5$– $30ZnO$–$10K_2O$–$5Al_2O_3)_{100-x}+xNd_2O_3$ ($x=0.25$, 0.5, 1.0, 1.5, 2.0 and 4.0) (in mol. %) were studied. Here, Nd_2O_3 was employed to finely tune the specific thermal and optical properties of the glass in view of core and clad fiber fabrication. The glasses were prepared by the standard melt-quenching technique. High purity (99.999%) precursors (H_3PO_4, ZnO, K_2CO_3, Al_2O_3, and Nd_2O_3) were ground and placed together in a platinum crucible and melted at 1100 °C for several hours. Stirring and grinding operations were performed during the synthesis to improve glass homogeneity. 8 mm diameter and ~ 6 cm long mono-material glass rods were fabricated from ~ 15 g batches. After quenching, the samples were annealed at 10 °C below their glass transition temperature for 8 h to reduce internal stress. Glass slabs of a few millimeter-thick each were cut from the cylindrical preforms and subsequently polished for optical characterizations.

The glass preforms were drawn under an Ar flow (2 L/min) using a dedicated 3 m high draw tower at ~ 560 °C–600 °C. First the macroscopic arrangement was heated up to its softening temperature at 10 °C/min to initiate the elongation process. After that, the preform was slowly fed into the furnace while the drawing parameters were continuously monitored to produce a fiber with a constant outer diameter and thus ensuring the uniformity of the profile along the fiber length. Further experimental details are provided below regarding the assembling of the preforms and their drawing into neodymium-doped multimode fibers.

2.2 Thermal and physical properties

The glass transition temperature (T_g) and crystallization temperature (T_c) were determined through differential scanning calorimetry (DSC) measurements with precision of ± 3 °C. DSC curves of ~ 60 mg glass samples were registered between 20 °C and 700 °C with a heating rate of 10 °C/min under ambient air. T_g was taken at the inflection point of the endotherm, as obtained by taking the first derivative of the DSC curve. T_c is defined as the onset of the exothermic peak.

The density of the bulk glass materials was determined through Archimedes' method in Diethyl phthalate. The precision was better than ± 0.02 g/cm^3.

2.3 Optical properties

Refractive indices were measured at 656 nm using Abbe refractometer (Atago). Optical loss measurements were carried out using the cutback method on fiber samples of several meters each. A 1310 nm laser source, with power of a few mW, was coupled into the phosphate fiber by the means of a silica objective (20 × and 0.32 NA). The output power was then measured for different sample lengths using a power-meter with μW sensitivity.

2.4 Nonlinear experiments configuration

SC generation was obtained by pumping the multimode rectangular-core phosphate fiber with a 1030 nm laser source delivering 250 fs pulses at a repetition rate of 300 kHz with a maximum average power of 2 W. The laser beam was coupled to the phosphate waveguides using a convergent lens ($f=175$ mm) (coupling efficiency estimated to ~ 50%). The generated spectral broadenings were collected by directly aligning the output of the phosphate fiber samples with a

multimode silica collection fiber. The signal was then analyzed with an optical spectrum analyzer operating in the 350–1750 nm range.

3 Results and discussion

3.1 Material development

Here, we chose the P_2O_5–ZnO–K_2O–Al_2O_3 system for multimode step-index fiber development. Often phosphate vitreous materials suffer from poor mechanical properties and low chemical resistance, especially against exposure to humidity. However, when tailored with the appropriated addition of oxide compounds, phosphate glasses have proven to form vitreous matrices suitable for optical fiber development, with good chemical durability and excellent shaping ability [14, 15]. Presence of the network intermediate Al_2O_3 increases the glass stability [29] and reduces rare-earth ions clustering [30] while ZnO helps preventing devitrification [31, 32]. It is worth noting that the alkali metal oxide K_2O was added, in the work reported in this paper, to lower the glass characteristic temperatures (glass transition and melting temperatures) for better rare earth oxide solubility and easier performance of shaping.

Glasses of composition $(55P_2O_5–30ZnO–10K_2O–5Al_2O_3)_{100-x}+xNd_2O_3$ ($x=0.25$ to 4.0) were synthesized here, and their main properties are summarized in Table 1.

Evolution of the glass transition temperature with respect to neodymium oxide content is plotted in Fig. 1a. It reveals that addition of Nd_2O_3 changed the thermal characteristics of the host zinc-phosphate glass. The glass transition temperature indeed gradually increased with higher neodymium oxide content. This indicates that neodymium ions brought greater rigidity and connectivity to the glassy network by increasing cross-linking in a similar fashion as is achieved by using aluminum oxide [29]. No crystallization temperature was visible at the 10 °C/min measurements rate for the different samples, except for the 2.0% and 4.0%, confirming the good stability of the host matrix. All glass samples exhibit T_c-T_g differences greater than 100 °C and are therefore thermally suitable for fiber drawing.

A picture of the samples investigated here is shown in Fig. 1b. The gradual coloration of the glass is due to the multiple visible absorptions related to $4f^3$ transitions of neodymium [33, 34]. The samples showed good homogeneity and overall fine neodymium incorporation even for important doping levels. High solubility of rare-earth ions is one of the major assets of use of phosphate glasses. It ensured good pump conversion over short propagation distances and could further allow the development of extremely compact, short laser systems.

As expected, the glass density increased with the addition of Nd_2O_3, which possesses a high molar mass (336.48 g/mol) as compared to the calculated host matrix molar mass (117.01 g/mol). The refractive index followed a comparable linear trend as depicted in Fig. 1c. It increased from 1.528 for the undoped glass up to 1.540 for the sample containing the highest Nd_2O_3 proportion. Addition of Nd^{3+} ions led to the presence of more non-bridging oxygen atoms within the glass matrix, producing an increase of electron polarizability [35].

Evolution of the index is of great interest for step-index optical fiber manufacturing which needs fine control of refractive index difference between the core and the cladding materials. This is especially true for laser applications which require on one hand large cores to increase the available output power, but on the other hand low numerical aperture (NA) to keep the single- or quasi single-mode operation and guaranty satisfactory beam quality. Here, when considering the undoped and Nd-loaded glasses as respectively cladding and core materials, the Nd_2O_3 concentration could be set to target specific refractive index steps for the final fiber.

Table 1 Physicochemical properties of the glasses in the system $(55P_2O_5–30ZnO–10K_2O–5Al_2O_3)_{100-x}+xNd_2O_3$ ($x=0.25$, 0.5, 1.0, 1.5, 2.0 and 4.0) (in mol. %)

Nd_2O_3 doping		T_g	T_c	ΔT	Density	$[Nd^{3+}]$	$n_{@656\ nm}$
/(mol. %)	/(wt. %)	/±3 °C	/±3 °C	/±6 °C	/±0.02(g·cm^{-3})	/(10^{20} ions·cm^{-3})	(±0.001)
0	0	417	n.m.	>283	2.80	0	1.528
0.25	0.72	420	n.m.	>280	2.82	0.72	1.531
0.5	1.42	422	n.m.	>278	2.85	1.45	1.532
1.0	2.82	430	n.m.	>270	2.88	2.91	1.533
1.5	4.20	435	n.m.	>265	2.89	4.34	1.535
2.0	5.54	438	555	117	2.90	5.75	1.536
4.0	10.70	456	590	134	2.95	11.30	1.540

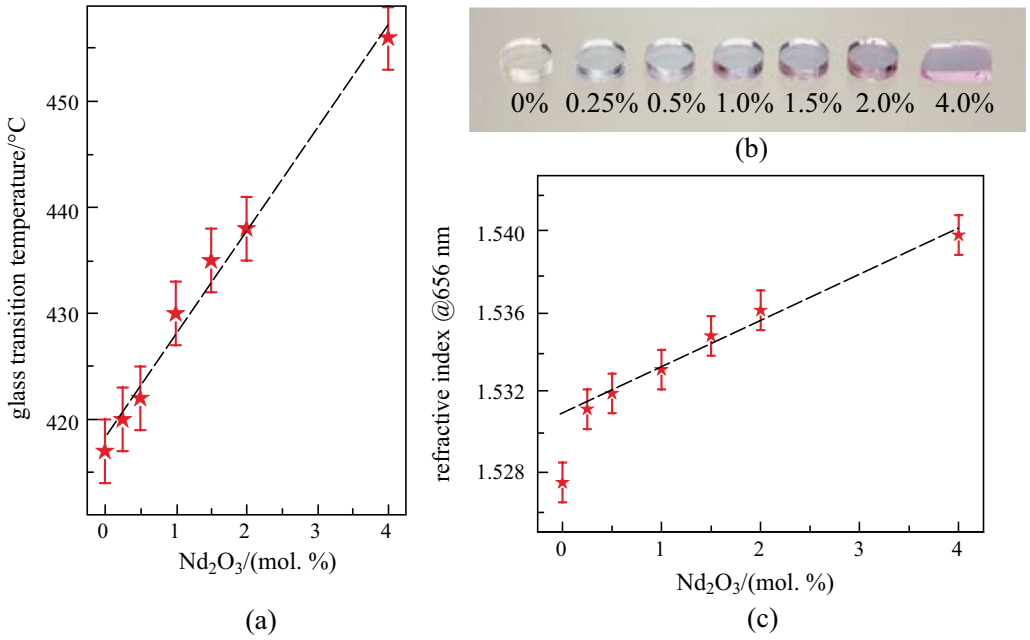

Fig. 1 Evolution of **a** glass transition temperature, **b** glass samples, and **c** refractive index at 656 nm as function of Nd_2O_3 doping level (in mol. %)

3.2 Neodymium-doped multimode fiber fabrication

In a first step, a cylindrical multimode fiber (MMF) was fabricated by exploiting the vitreous materials developed in the previous section. A large-core preform was manufactured using the built-in casting method [36]. The undoped glass was chosen for the cladding material while the glass doped with 1.0 mol. % Nd_2O_3 was selected for the core. A cross-sectional view of a typical step-index rod is presented in Fig. 2b. The refractive index difference between the core and the cladding was $(5 \pm 2) \times 10^{-3}$ (at 656 nm) and the glass transition temperature difference $\Delta T_g = (13 \pm 6)$ °C, meaning the two glasses were thermally and optically compatible for fiber development. The preform was then stretched down in homothetic fashion to a multi-mode fiber for further characterizations. A cross-sectional view of the as-drawn MMF is presented in Fig. 2c. No index fluctuation (glass striae) was visible on the fiber microscope pictures taken

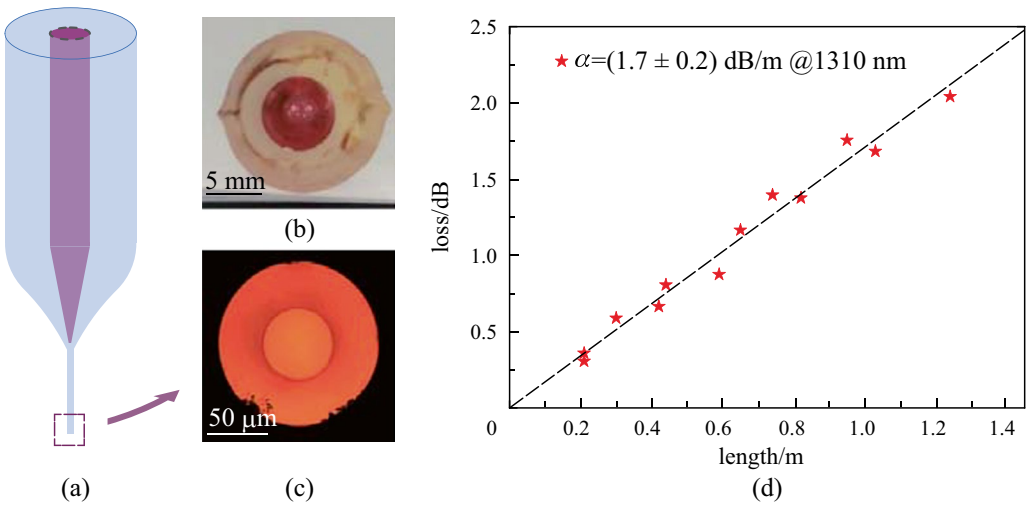

Fig. 2 **a** Thermal drawing of a large-core cylindrical phosphate fiber. Cross-sectional view of **b** step-index glass preform and **c** neodymium-doped multimode fiber. **d** Optical loss of the MMF measured at 1310 nm

in transmission mode, which attests good homogeneity of the core glass. Additionally, the structure possessed a good core-cladding interface without particular defects (bubbles, crystallites, etc.). Those observations were confirmed by the attenuation at 1310 nm which was found to be as low as 1.7 dB/m (see Fig. 2d). It is worth noting that this value was comparable to the attenuation measured on single-index cylindrical fibers made from the cladding or core glass (respectively 1.4 and 1.8 dB/m). The properties of this cylindrical MMF are summarized in Table 2.

The development of multi-mode cylindrical waveguides allowed assessment of the ability of the phosphate glass to be shaped into fibers of optical quality. Regarding the direct preform-to-fiber fabrication of a rectangular-core fiber, we selected the glass doped with 1.5% neodymium oxide as the core material because of its high Nd_2O_3 content combined with its excellent thermal stability. The undoped glass was chosen as the cladding material. The refractive index difference between the core and the cladding was $(7 \pm 2) \times 10^{-3}$ (at 656 nm), producing a fiber with a numerical aperture of 0.15. The core and the cladding both exhibited T_c–T_g differences greater than 100 °C and were therefore thermally suitable for fiber drawing. Additionally, they showed a moderate glass transition temperature difference $\Delta T_g = (18 \pm 6)$ °C, meaning they were thermally compatible for co-drawing. Again, optical loss measurements were carried out on single-index cylindrical fibers to verify the optical quality of the core material doped with 1.5 mol. % Nd_2O_3 (Table 2). A moderate attenuation of 1.9 dB/m was measured at 1310 nm, which was sufficient for the nonlinear experiments described below, involving short fiber segments.

Then, a glass preform possessing a rectangular core was fabricated using a modified stack-and-draw technique as outlined in Fig. 3 [28].

The different parts of the preform were cut out from glass rods and plates fabricated with the melt-quenching technique. Two half-cylinders and three rectangular canes were used here (see Fig. 3a). Those parts were then carefully polished to produce high quality surfaces and put together to form the preform. The assembly was then annealed for two hours at $T_g + 50$ °C while a moderate pressure (few kPa) was applied to the glass pieces by means of ceramic weights. This step allowed for the bonding of the different glass parts and ensured good and permanent contact between them. This procedure, also known as fusion bonding, is widely used with silicate glasses in microfluidics for micro-chip assembly or for silicon wafer assembly [37]. The glass pieces bond together as a result of a reaction between the Si–OH groups existing at the surface of the slabs. Upon heating, H_2O is released while Si–O–Si entities form, bonding the glasses together [38]. In the present case, P-OH or M-OH (M for cations) present at the surface of the phosphate glasses reacted

Table 2 Properties of the P_2O_5-based multimode fibers (MMF) investigated in this section

	Nd_2O_3 core doping /(mol. %)	ΔT_g (±6)/°C	$\Delta n_{@656\,nm}$ (±0.002)	Optical loss at 1310 nm/(dB·m^{-1})		
				Cladding	Core	MMF
Cylindrical MMF	1	13	$5 \cdot 10^{-3}$	1.4	1.8	1.7
Rectangular MMF	1.5	18	$7 \cdot 10^{-3}$	1.4	1.9	14*

* Optical loss measured at 1030 nm

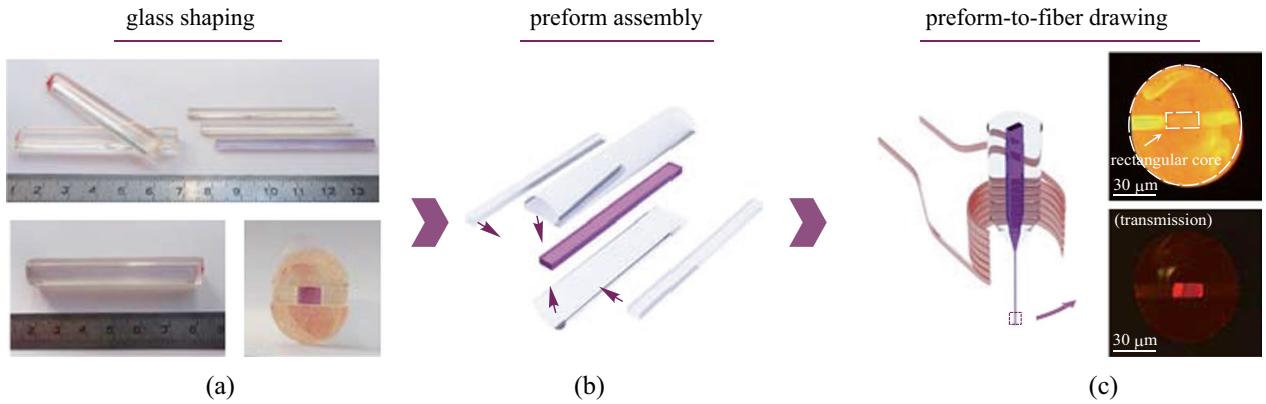

Fig. 3 **a** Pictures of the different phosphate glass parts used for the preform design. **b** Description of the preform assembly and **c** thermal drawing of rectangular-core phosphate fibers

when heated up, releasing molecular water and forming P-O-P or P-O-M bonds, bridging the glass pieces together. This procedure is of great importance for fiber drawing as it gives the needed cohesion to the preform built from the different glass pieces. After that, the preform was thermally scaled down in a homothetic fashion to produce tens-of-meter long rectangular-core optical fibers. Light guiding inside the non-cylindrical core of the produced wave-guide was assessed as shown in Fig. 3b.

3.3 Supercontinuum generation

A fiber with a rectangular-core of 30 µm in thickness to 60 µm in width was fabricated following the method described previously. The number of supported modes at 1030 nm was estimated at ~ 95 in such a structure. Thus, the purpose of the first experiment was to observe the output beam shape at the fiber end after the coupling of a 1030 nm Gaussian beam with 25 µm diameter (see Fig. 4a). In these conditions, the input coupling could select different groups of modes in order to provide different output beam patterns. In this case, the selection of a low number of modes was possible, leading to the reduction of the output speckle (see inset of Fig. 4a). The optical loss in the fiber was measured by using the cut-back technique and was estimated to be close to 14 dB/m, which was well above the values determined on single-index fibers or on the cylindrical MFF (see Table 2). That high coefficient most probably originated from poor core-cladding interfaces where diffusion centers (glass stria, interface imperfections, bubbles) could form during the thermal drawing. In particular, when comparing this value to the 1.7 dB/m attenuation measured on the cylindrical MMF, it appeared that the high optical loss measured on the rectangular-core fiber did not derive from poor material quality but rather from the waveguide geometry and the preform manufacturing process. Further improvement, including optimization of the fabrication protocol and modeling to optimize the geometry of the rectangular core must be considered in order to lower the loss value.

In the second step we investigated the supercontinuum generation by using femtosecond pulses. To counterbalance the dispersion and the group velocity difference between modes, the peak power was significantly increased in order to reach the self-focusing propagation regime (Figs. 4 and 5). In these conditions, the first nonlinear signature appeared in the spatial domain with nonlinear self-focusing which significantly changed the spatial beam pattern and drastically improved the local power density inside the fiber. The nonlinear multimode filament was perfectly guided in the fiber core and underwent spatial reorientation because of the nonlinear interactions between transverse modes supporting different energies. Thus, the linear refraction process, well known in the optical fiber, was no longer conserved and nonlinear reflection could be observed. Figure 4b shows an example of that process with a quasi-total reflection at the core cladding interface, changing an incident angle of 21° into an output one close to only 8°. This atypical process had a strong influence on the beam propagation and also on the frequency conversion. The nonlinear propagation regime was observed on the side of the optical fiber because of non-collinear frequency conversion obtained on leaky modes and by means of a Cerenkov phase-matching process. The signature of that non colinear conversion was clearly visible on the far field image of the converted output beam with a thin ring surrounding the main central spot (Fig. 4c). However, because of the high numerical aperture of the fiber, a large part of the converted beam was collected on the central beam, constituted of several transverse modes. After a given propagation length, the impact of the nonlinearity reached a critical level and broke the initial white filament (see Fig. 5a–f). Thus, a nonlinear frequency conversion could be obtained in the infrared domain by using self-phase modulation and the Raman effect.

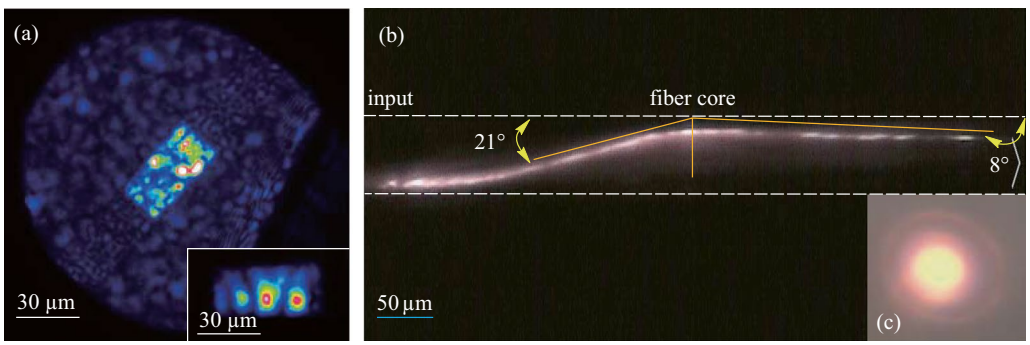

Fig. 4 **a** Image of the output beam at the fiber end. The guided zone is estimated to 30/60 µm; Inset: example of excitation of few modes by controlling the input coupling. **b** Nonlinear propagation of the incident beam inside the core fiber and leading to nonlinear refraction evolution (Input peak power: 1.6 MW). **c** Far field image of the output visible beam for peak power of 2 MW

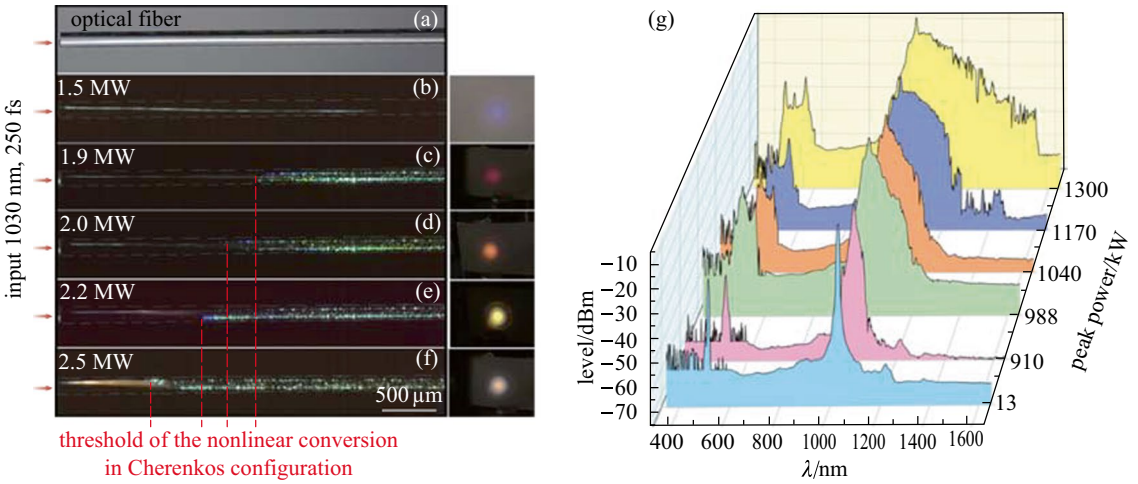

Fig. 5 Longitudinal view of the rectangular fiber during nonlinear conversion process versus the input peak power. Fiber without pumping **a**, fiber pumped at 1030 nm, 250 fs versus input peak power **b**–**f**. Insets on the right side of the figure correspond to the output beam pattern observed in the visible domain after 45 cm of propagation. **g** Spectrum recorded at the fiber end versus the input peak power

A supercontinuum up to 1550 nm was observed for a peak power close to 1.9 MW (Fig. 5c). The conversion toward the visible region was first obtained, in part, by second harmonic generation (SHG) at 515 nm and was followed by four-wave mixing processes which enlarged the visible spectrum (Fig. 5g). The phase matching process regarding the SHG was obtained thanks to non colinear phase matching configuration [39, 40]. Phase matching of additional v was mainly obtained by modal mixing. The higher the input power, the earlier the nonlinear conversion appeared in the optical fiber (see Fig. 5b–f).

4 Conclusions

A detailed study concerning the development of zinc-phosphate glasses doped with different Nd_2O_3 concentrations was carried out. Linear evolution of the glass properties (glass transition temperature and refractive index) with respect to Neodymium oxide concentration was observed. Then, thanks to the good fiber drawing ability of the developed glasses, multimode large rectangular-core fibers were produced by a modified stack-and-draw method. Self-guided nonlinear effects, acting as a spatial beam reshaping which concentrated the input energy, facilitated large-band frequency conversion in the visible and infrared domains in this new waveguide structures. An additional spatial routing of self-focused filament due to interplay between multimode propagation and nonlinearity was also observed. Further work will be devoted to determine whether the nonlinear dynamics exploited here are compatible with gain in the fiber.

Acknowledgements Funding for this work has been provided from the French Government, managed by the French National Research Agency (ANR Grant #62,243), by the Program IdEx at the University of Bordeaux, the Cluster of excellence LAPHIA and by the Région Nouvelle-Aquitaine. We also acknowledge the financial support provided by CILAS Company (ArianeGroup) through the shared X-LAS laboratory.

Authors' contributions All authors have read and approved the final manuscript.

Declarations

Competing interests The authors declare that they have no competing interests.

References

1. Krupa, K., Tonello, A., Shalaby, B.M., Fabert, M., Barthélémy, A., Millot, G., Wabnitz, S., Couderc, V.: Spatial beam self-cleaning in multimode fibres. Nat. Photonics **11**(4), 237–241 (2017)
2. Guenard, R., Krupa, K., Dupiol, R., Fabert, M., Bendahmane, A., Kermene, V., Desfarges-Berthelemot, A., Auguste, J.L., Tonello, A., Barthélémy, A., Millot, G., Wabnitz, S., Couderc, V.: Kerr self-cleaning of pulsed beam in an ytterbium doped multimode fiber. Opt. Express **25**(5), 4783–4792 (2017)
3. Krupa, K., Louot, C., Couderc, V., Fabert, M., Guenard, R., Shalaby, B.M., Tonello, A., Pagnoux, D., Leproux, P., Bendahmane, A., Dupiol, R., Millot, G., Wabnitz, S.: Spatiotemporal characterization of supercontinuum extending from the visible to the mid-infrared in a multimode graded-index optical fiber. Opt. Lett. **41**(24), 5785–5788 (2016)
4. Lopez-Galmiche, G., Eznaveh, Z.S., Eftethkhar, A., Antonio-Lopez, J., Wise, F., Christodoulides, D., Correa, R.A.: Visible supercontinuum generation in a low DGD graded index multimode fiber. 2016 Conf. Lasers Electro-Optics, CLEO **2016**(41), 2553–2556 (2016)
5. Alfano, R.R., Shapiro, S.L.: Emission in the region 4000 to 7000 Å via four-photon couplingin glass. Phys. Rev. Lett. **24**(11), 584–587 (1970)
6. Ranka, J.K., Windeler, R.S., Stentz, A.J.: Visible continuum generation in air-silica microstructure optical fibers with anomalous dispersion at 800 nm. Opt. Lett. **25**(1), 25–27 (2000)
7. Dudley, J.M., Provino, L., Grossard, N., Maillotte, H., Windeler, R.S., Eggleton, B.J., Coen, S.: Supercontinuum generation in air–silica microstructured fibers with nanosecond and femtosecond pulse pumping. J. Opt. Soc. Am. **19**(4), 765 (2002)
8. Kudlinski, A., Bouwmans, G., Vanvincq, O., Quiquempois, Y., Le Rouge, A., Bigot, L., Mélin, G., Mussot, A.: White-light cw-pumped supercontinuum generation in highly GeO_2-doped-core photonic crystal fibers. Opt. Lett. **34**(23), 3631–3633 (2009)
9. Dudley, J.M., Genty, G., Coen, S.: Supercontinuum generation in photonic crystal fiber. Rev. Mod. Phys. **78**(4), 1135–1184 (2006)
10. Bullington, A.L., Pax, P.H., Sridharan, A.K., Heebner, J.E., Messerly, M.J., Dawson, J.W.: Mode conversion in rectangular-core optical fibers. Appl. Opt. **51**(1), 84–88 (2012)
11. Modotto, D., De Angelis, C., Magaña-Cervantes, M.A., De La Rue, R.M., Morandotti, R., Linden, S., van Driel, H.M., Aitchison, J.S.: From linear to cubic nonlinear imaging effects in multimode waveguides. J. Opt. Soc. Am. **22**(4), 870 (2005)
12. Li, W.L., Chen, D.C., Zhou, Q.Z., Hu, L.H.: Watt-level output rectangular-core neodymium-doped silicate glass fiber laser. Chin. Opt. Lett. **14**(1), 011402–011404 (2016)
13. Drachenberg, D.R., Messerly, M.J., Pax, P.H., Sridharan, A.K., Tassano, J.B., Dawson, J.W.: Yb^{3+} doped ribbon fiber for high-average power lasers and amplifiers. In: Fiber Lasers XI: Technology, Systems, and Applications (SPIE, 2014), Vol. 8961, p. 89610T.
14. Mura, E., Lousteau, J., Milanese, D., Abrate, S., Sglavo, V.M.: Phosphate glasses for optical fibers: Synthesis, characterizationand mechanical properties. J. Non-Cryst. Solids **362**, 147–151 (2013)
15. Danto, S., Désévédavy, F., Petit, Y., Desmoulin, J.C., Abou Khalil, A., Strutynski, C., Dussauze, M., Smektala, F., Cardinal, T., Canioni, L.: Photowritable silver-containing phosphate glass ribbon fibers. Adv. Opt. Mater. **4**(1), 162–168 (2016)
16. Lee, Y.W., Sinha, S., Digonnet, M.J.F., Byer, R.L., Jiang, S.: Measurement of high photodarkening resistance in heavily Yb^{3+}-dopedphosphate fibres. Electron. Lett. **44**(1), 14–16 (2008)
17. Shi, W., Petersen, E.B., Yao, Z., Nguyen, D.T., Zong, J., Stephen, M.A., Chavez-Pirson, A., Peyghambarian, N.: Kilowatt-level stimulated-Brillouin-scattering-threshold monolithic transform-limited 100 ns pulsed fiber laser at 1530 nm. Opt. Lett. **35**(14), 2418–2420 (2010)
18. Boetti, N., Pugliese, D., Ceci-Ginistrelli, E., Lousteau, J., Janner, D., Milanese, D.: Highly doped phosphate glass fibers for compact lasers and amplifiers: a review. Appl. Sci. **7**(12), 1295 (2017)
19. Schülzgen, A., Zhu, X., Temyanko, V.L., Peyghambarian, N., Li, L., Li, L.: Microstructured active phosphate glass fibers for fiber lasers. J. Lightwave Technol. **27**(11), 1734–1740 (2009)
20. Lee, Y.W., Digonnet, M.J.F., Sinha, S., Urbanek, K.E., Byer, R.L., Jiang, S.: High-power Yb^{3+}-doped phosphate fiber amplifier. IEEE J. Sel. Top. Quantum Electron. **15**(1), 93–102 (2009)
21. Wang, C., Lin, Z., Zhang, L., Chen, D.: Single-mode laser output in a Yb^{3+}-doped fluorophosphate fiber. J. Opt. Soc. Am. B: Opt. Phys. **33**(9), 1796–1799 (2016)
22. Thapa, R., Nguyen, D., Zong, J., Chavez-Pirson, A.: All-fiber fundamentally mode-locked 12 GHz laser oscillator based on an Er/Yb-doped phosphate glass fiber. Opt. Lett. **39**(6), 1418–1421 (2014)
23. Shi, W., Petersen, E.B., Leigh, M., Zong, J., Yao, Z., Chavez-Pirson, A., Peyghambarian, N.: High-energy single-mode single-frequency all-fiber laser pulses coveringC-band based on highly co-doped phosphate glass fibers. Proc. SPIE **7195**, 71951H-H71961 (2009)
24. Akbulut, M., Miller, A., Wiersma, K., Zong, J., Rhonehouse, D., Nguyen, D., Chavez-Pirson, A.: High energy, high average and peak power Phosphate-Glass fiber amplifiersfor 1micron band. In: SPIE LASE, pp. 89611X–89611X (2014)
25. Rota-Rodrigo, S., Gouhier, B., Laroche, M., Zhao, J., Canuel, B., Bertoldi, A., Bouyer, P., Traynor, N., Cadier, B., Robin, T., Santarelli, G.: Watt-level single-frequency tunable neodymium MOPA fiber laser operating at 915–937 nm. Opt. Lett. **42**(21), 4557–4560 (2017)
26. Campbell, J.H., Suratwala, T.I., Thorsness, C.B., Hayden, J.S., Thorne, A.J., Cimino, J.M., Marker, A.J.I.I.I., Takeuchi, K., Smolley, M., Ficini-Dorn, G.F.: Continuous melting of phosphate laser glasses. J. Non-Cryst. Solids **263**, 342–357 (2000)
27. Fu, S., Zhu, X., Zong, J., Li, M., Zavala, I., Temyanko, V., Chavez-Pirson, A., Norwood, R.A., Peyghambarian, N.: Single-frequency Nd^{3+}-doped phosphate fiber laser at 915 nm. J. Lightwave Technol. **39**, 1808–1813 (2021)
28. Strutynski, C., Meza, R.A., Teulé-Gay, L., El-Dib, G., Poulon-Quintin, A., Salvetat, J., Vellutini, L., Dussauze, M., Cardinal, T., Danto, S.: Stack-and-draw applied to the engineering of multi-material fibers with non-cylindrical profiles. Adv. Func. Mater. **31**(22), 2011063 (2021)
29. Bingham, P.A., Hand, R.J., Forder, S.D.: Doping of iron phosphate glasses with Al_2O_3, SiO_2 or B_2O_3 for improved thermal stability. Mater. Res. Bull. **41**(9), 1622–1630 (2006)
30. Cole, J.M., Van Eck, E.R.H., Mountjoy, G., Anderson, R., Brennan, T., Bushnell-Wye, G., Newport, R.J., Saunders, G.A.: An X-ray diffraction and 31P MAS NMR study of rare-earth phosphate glasses,($R_2O_3)_x(P_2O_5)_{1-x}$, $x = 0.175–0.263$, R = La, Ce, Pr, Nd, Sm, Eu, Gd, Tb, Dy, Ho. Er. J. Phys. Conden. Matter **13**(18), 4105–4122 (2001)
31. Aida, K., Komatsu, T., Dimitrov, V.: Thermal stability, electronic polarisability and optical basicity of ternary tellurite glasses. Phys. Chem. Glasses **42**, 103–111 (2001)
32. Musinu, M., Piccaluga, G., Magini, M.: Coordination of Zinc (II) in ZnO-K_2O-SiO_2 Glasses by X-ray Diffraction. J. Am. Ceram. Soc. **71**(5), 256 (1988)
33. Campbell, J.H., Suratwala, T.I.: Nd-doped phosphate glasses for high-energy/high-peak-power lasers. J. Non-Cryst. Solids **263**, 318–341 (2000)
34. Caird, J.A., Ramponi, A.J., Staver, P.R.: Quantum efficiency and excited-state relaxation dynamics in neodymium-dopedphosphate laser glasses. J. Opt. Soc. Am. **8**(7), 1391–1403 (1991)
35. Algradee, M.A., Sultan, M., Samir, O.M., Alwany, A.E.B.: Electronic polarizability, optical basicity and interaction parameter

for Nd_2O_3 doped lithium–zinc–phosphate glasses. Appl. Phys. A Mater. Sci. Process. **123**(8), 524 (2017)
36. Strutynski, C., Picot-Clémente, J., Lemiere, A., Froidevaux, P., Désévédavy, F., Gadret, G., Jules, J.C., Kibler, B., Smektala, F.: Fabrication and characterization of step-index tellurite fibers with-varying numerical aperture for near- and mid-infrared nonlinear optics. J. Opt. Soc. Am. B: Opt. Phys. **33**, D12–D18 (2016)
37. Fan, Z.H., Harrison, D.J.: Micromachining of capillary electrophoresis injectors and separators on glass chips and evaluation of flow at capillary intersections. Anal. Chem. **66**(1), 177–184 (1994)
38. Berthold, A., Jakoby, B., Vellekoop, M.J.: Wafer-to-wafer fusion bonding of oxidized silicon to silicon at low temperatures. Sens. Actuators **68**(1–3), 410–413 (1998)
39. Cerenkov, P.: Visible glow under exposure of gamma-radiation. Dokl. Akad. Nauk SSSR **2**, 451 (1934)
40. Saltiel, S.M., Sheng, Y., Voloch-Bloch, N., Neshev, D.N., Krolikowski, W., Arie, A., Koynov, K., Kivshar, Y.S.: Cerenkov-type second-harmonic generation in two-dimensional nonlinear photonic structures. IEEE J. Quantum Electron. **45**(11), 1465–1472 (2009)

Clément Strutynski is a research associate in the Soliton, Lasers and Optical Communications (SLCO) group at Carnot Interdisciplinary Laboratory of Burgundy (ICB), Dijon, France. He received his Ph.D. degree in Materials Physics from the University of Burgundy, France. During his thesis work, he developed all solid and micro structured fibers from highly purified Tellurite glasses for supercontinuum generation in the mid-infrared. During the period of 2016/6–2020/9, he was a research associate in the Institute of Chemistry of the Condensed Matter of Bordeaux (ICMCB), Pessac, France. There, his activities were focused on the design of unique all-glass or polymer/glass/metal elongated structures for sensing or Laser applications. His current research interests include glass science, fiber design and fabrication as well as multi-material fibers.

Vincent Couderc received his Ph.D. degree from the University of Limoges, France. He joined the National Center for Scientific Research (CNRS) in 1996 and is today Research Director. He currently heads the "Biophotonics" group at the XLIM Research Institute (Limoges, France). His research interests include nonlinear propagation in crystals and optical fibers, soliton propagation, diode pumped laser sources, nonlinear optical complexities, nonlinear frequency conversion, and optoelectronic switching. He is a member of the French Optical Society.

Tigran Mansuryan received his Ph.D. degree in Laser Physics in 2008 from the Physics Department of Yerevan State University. During the period 2009–2014 he was a post-doctoral researcher at XLIM, Limoges University, France. From 2014 to 2018 he was a R&D engineer at KAMAX Innovative System. He is now a researcher in XLIM, Limoges University. His research focuses on nonlinear-optical methods of microscopy, fiber endoscopy, fiber non-linearity, ultrafast optics, femtosecond technologies.

Giorgio Santarelli received his Ph.D. degree from the Université Pierre et Marie Curie (Paris VI, France) in 1996. Since 1991 he has been research staff in the LNE-SYRTE, Observatoire de Paris. In 2012, G. Santarelli joined the LP2N research laboratory in the Bordeaux area. Dr. G. Santarelli is Top-Tiers CNRS Research Engineer (IRHC) at LP2N. His research interests are in high power low noise lasers, novel laser sources, ultra-stable lasers, femtosecond laser combs, very low phase noise frequency synthesis, cold atoms frequency standards and long distance fibre optical frequency dissemination. He is the author of more than 120 peer reviewed technical articles, 2 patents and 3 book chapters and several oral presentations in international conferences and invited talks. He is also Associate Editor in Chief of the IEEE Transactions on Ultrasonics, Ferroelectrics and Frequency Control and has served as Chair the Executive Committee of the European Frequency and Time Forum. Dr. G. Santarelli received the 2015 the "European Frequency and Time" Award for his outstanding contributions to the development of ultra-low phase noise methods and systems for microwave and optical atomic clocks, fibre-based optical frequency combs and optical fibre links. He established at the LP2N a shared lab with an industrial partner leader in high power fibre laser development (Azur Light Systems). He is also the co-founder of a start-up company (Irisiôme) developing innovative pulsed lasers systems for medical/dermatological applications.

Philippe Thomas received his Ph.D. degree in 1989 from the University of Limoges in the field of ceramic processes and surface treatments. He was then employed as Project Leader in General Electric Company from 1989 to 1991 and then joined the National Center for Scientific Research (CNRS) as a researcher at the Institute of Research for Ceramics (IRCER) in Limoges, France. He was appointed Director of Research at the CNRS in 2004. From 2006 to 2017, he

was the head of the "Multi-scale structural organisation of materials" team at IRCER. During the year 2017, he was the Deputy Director of IRCER and since 2018, he is the Director of IRCER. He is involved (01/2019–12/2023) in the scientific management of an International Research Project CNRS, "Ceramics materials for societal challenges", between IRCER and the National Institute of Technology of Nagoya (Japan). His main research interest concerns (i) Oxide materials based on elements possessing a lone electronic pair ns2 (such as Te^{4+}, Tl^{+}, Bi^{3+}, Pb^{2+}); (ii) Crystal chemistry and optical characterization of vitreous and crystalline compounds; (iii) New tellurium oxide-based materials (crystals and glasses) for nonlinear optics; (iv) *Ab initio* modelling of the hyper-polarizability of tellurite materials; (v) Metal oxide nanoparticles. He has co-authored 167 peer-reviewed papers and 6 patents. He has been the supervisor of 26 graduated PhD students and has given 44 invited talks. He has been involved in 22 academic projects and industrial projects including international ones, mostly as coordinator.

Sylvain Danto received his Ph.D. degree in Materials Science from the University of Rennes (Rennes, France) in 2005 where he worked on amorphous semiconductors for data storage and infrared optics. Next he joined the group of the Prof. Yoel Fink at the Massachusetts Institute of Technology (MIT), Cambridge, USA, as a research associate (2006–2010). At MIT he developed novel multi-material optical fibers for optoelectronic devices. Then he joined the group of the Prof. Kathleen Richardson at Clemson University, USA, as a research scientist (2011–2013). There he pursued research on amorphous semiconductors for mid-infrared optics and photonics, in bulk, film and fiber forms. Currently he is located at the Institute of Chemistry of the Condensed Matter of Bordeaux (ICMCB, UMR 5026 CNRS University of Bordeaux). There he aims at establishing a new research activity and dedicated facility on soft-Tg-glass-based specialty optical fibers for applications ranging mid-infrared optics, photosensitive fibers, fiber Lasers and novel smart fibers with unique functionalities. Dr. S. Danto is coauthor of more than 40 journal publications, 2 book-chapters and he holds 4 patents on optical glasses and fibers.

Thierry Cardinal received his Ph.D. degree in Oxide Glass for Nonlinear Optics at Bordeaux 1 University in 1997. After a stay at University of Central Florida, he was appointed at CNRS at ICMCB (University of Bordeaux) in 1998. His interests are on exotic glass and glass ceramic compositions for nonlinear optics, nano-structured materials, poling, luminescence and Direct Laser Writing processes and photochemistry in photosensitive glasses. He has investigated nonlinear optical properties in glass (Kerr effect and Raman Gain). He is developing in University of Bordeaux a research programs on 3D printing, and specialty fibers. He has been co-authored about 155 publications in peer reviewed journals. He holds 7 patents, with 1 license. He has been coordinator or participant of several academic research programs (ACI, ANR, CNRS, Europe, "Nouvelle Aquitaine" region) in the field of novel photonic materials. Thierry Cardinal is director of the IRP LUMAQ gathering research teams working on photonics and Lasers between University of Bordeaux in France, Laval University and INRS in Canada.